ORIGINAL PAPER

Face failure mechanism of shield tunnel in sandy ground with different low moisture contents

Zhongrong Wang[1] · Wantao Ding[1,2] · Xinghang Huang[1] · Rui Chen[1] · Keqi Liu[3]

Abstract

Maintaining face stability of tunnels during tunnel excavation is essential. Studies on face stability of shield tunnels are generally conducted in completely dry or saturated sandy soils, and there are few studies on face stability in sandy ground with different low moisture contents. However, most practical conditions involve unsaturated sandy ground. In this regard, to investigate the tunnel face stability in sandy ground with different low moisture contents, a series of 1-g large-scale earth pressure balance (EPB) shield model tests were conducted. Variation of face support pressure, ground settlement, vertical stress, and soil arching effect in sand during the construction of shield tunnel was revealed. Furthermore, three kinds of failure mechanisms were proposed considering the soil arching effect and the range of ground settlement. The results show that the moisture content has a significant impact on the limit support pressure, the evolution of soil arching, and failure mechanisms. With the increasing moisture content, the ground settlement trough is wider, but the settlement value is smaller. And higher moisture content corresponds more significant soil arching effect. Moreover, the existence of soil arching makes limit face support pressure much smaller than the initial support pressure. Furthermore, based on three kinds of failure mechanisms constructed in this paper, theoretic approaches to estimate the limit support pressure and analyze face stability in sand with different moisture contents are proposed. Compared with the existing research results, failure mechanisms and empirical approaches proposed in this paper are more applicable to analyze tunnel face stability in sand with different low moisture contents, which is also closer to engineering practice.

Keywords Large-scale model tests · Low moisture content · Limit support pressure · Soil arching · Failure mechanisms

Introduction

During the process of underground space development, EPB shield has been widely used for its safety in construction, high mechanization, and small impact on the surrounding environment. However, face instability even surface collapse will occur when tunneling if the support pressure is insufficient. Thus, the acquisition of limit support pressure

for shield and the construction of failure modes for soils have become important research contents during shield construction.

Scholars at home and abroad have carried out a series of studies on face stability by using theoretical analysis, laboratory tests, and numerical simulation. In theoretical analysis, based on the assumption of stress field or velocity field, limit analysis method provides the theoretical basis for the calculation of limit support pressure. Broms and Bennermark (1967) first introduced the theory of limit analysis to solve the limit face support pressure, and they defined a stability ratio N to evaluate whether the tunnel face is stable or not. On this basis, Davis et al. (1980) constructed failure mechanisms of circular tunnel with three variable angles and four variable angles considering the rigid block theory. Then, the upper and lower solutions of tunnel instability were obtained. Furthermore, Mollon et al. (2010) constructed a translational multiblock failure modes using a spatial discretization technology; then, the optimal solutions of limit

Responsible Editor: Zeynal Abiddin Erguler

✉ Wantao Ding
   dingwantao@sdu.edu.cn

1   School of Qilu Transportation, Shandong University,
    Jinan 250002, Shandong, China

2   Geotechnical and Structural Engineering Research Center,
    Shandong University, Jinan 250061, China

3   School of Resource and Civil Engineering, Northeastern
    University, Shenyang 110819, China

support pressure in different strata were obtained. In addition, based on the slip line and limit analysis theories, Ding et al. (2019) presented a 4-variable multizone mechanism, which significantly improved the existing upper bound solutions. What is more, many scholars considered some factors, such as the tunnel shape (Zhang et al. 2020), anisotropy of soils (Li and Zhang 2020), construction method (Ding et al. 2021), seepage flow (Li et al. 2021) and the cohesion of soils (Ding et al. 2018; Zhang et al. 2015), that may make a difference on the construction of failure mechanisms and made a great progress compared with the researches in the past.

Laboratory testing is another useful tool to carry out tunnel face stability analysis (Soranzo et al. 2015). Chambon and Corté (1994) performed centrifugal model tests to study the face stability in completely dry sandy ground. Zhou and Pu (2002) also conducted a series of centrifugal model tests to investigate the variation of support pressure and ground settlements during tunnel excavation in sands. Li et al. (2018) carried out a large-scale model test to investigate the face instability of shallow shield tunnels in sand. They discovered that there are three development stages of support pressure and surface deformation with the displacement of panel. Idinger et al. (2011) studied tunnel face stability by carrying out centrifuge tests. They found that arching effects were observed when $C/D = 1.0$ (C = buried depth and D = tunnel diameter). Li et al. (2011) and Chen et al. (2013) conducted 1-g large-scale model tests in dry sand for various C/D ratios to investigate the evolution of soil arching.

In addition, with the advancement of computing technology, numerical methods are increasingly providing a convenient environment for conducting tunnel face stability analysis (Satyanarayana et al. 2021; Liu et al. 2020a, b; Lin et al. 2019; Alagha and Chapman 2019). Lavasan et al. (2018) constructed a three-dimensional model to investigate the slurry shield tunneling in fully saturated soils. Ling et al. (2021) also conducted a series of numerical simulation of slurry shield tunnels, and they found the friction angle had a significant impact on the failure zone. Furthermore, some scholars have also applied discrete element method (DEM) to study tunnel face stability (Wang et al. 2019; Chen et al. 2011), and it was found that results obtained by numerical simulation were basically consistent with the model test results.

Most of the existing studies on face stability are conducted in completely dry or saturated sandy soils (Liu et al. 2018; Chen et al. 2018), while practical conditions mostly involve sandy ground with low moisture contents. And the construction of traditional failure mechanism of tunnel face does not consider the effect of different moisture contents on face stability, which will have a certain deviation from actual project. Therefore, it is more practical to consider the influence of different low moisture contents on face stability of shield tunnels in sandy ground. What is more,

existing research results (Chen et al. 2013; Liu et al. 2020a, b; Liu et al. 2021) show that soil arching effect will induce redistribution of stress in front of tunnel face, which will affect the face stability and ground settlement. However, when constructing the failure mechanism of tunnel face and solving the limit support pressure, the soil arching effect is often ignored. Hence, it is particularly important to study the evolution of soil arching effect.

In this paper, 1-g large-scale physical model tests of shield tunnels in sands with different low moisture contents ($\omega = 1.43\%$, 5.24%, and 9.3%) were carried out with $C/D = 1.0$. Firstly, the relationships between the support pressure and face displacement for various low moisture contents were discussed. Then, the influence of low moisture contents on the relevant parameters of the settlement trough was discussed, and the relationship between width coefficient of the settlement trough and moisture contents in sand with a certain range of moisture content was given. Next, the distribution of vertical earth pressure around the tunnel was analyzed, and the evolution characteristics of soil arching effect were discussed. Finally, considering the range of ground settlement and soil arching effect, three kinds of failure modes with three different low moisture contents were proposed, and the corresponding theoretic approach to estimate the limit support pressure and stability coefficient was obtained using the limit analysis method. Compared with the existing studies, the applicability of the presented model in sand with low moisture contents was verified. The research could provide some reference for the construction of failure mode and the prediction of limit support pressure in sandy ground with different low moisture contents.

Physical model test

Test apparatus

As shown in Fig. 1, the size of the model box was $2.4 \text{ m} \times 1 \text{ m} \times 2 \text{ m}$ (length × width × depth). The tunnel heading consisted of a 0.4-m-long and 10-mm-thick cylindrical steel shell with an inner diameter of 0.4 m. The tunnel face was a support plate which can be treated as rigid because of its high stiffness. The movement of the support plate was operated by a screw jack connected with the rotating shaft.

A load cell was set behind the support plate to measure support pressure of tunnel face. Twelve earth pressure cells were placed as shown in Fig. 2 to record soil stresses values, which were calibrated in order to register the stress during the tests. Seventeen LVDTs were placed on ground surface to measure the surface settlement, which were divided into three measuring lines (see Fig. 3), and at the tip of the probe for each LVDT, the contact plate was equipped. During the test, the screw rotated at a constant speed ($\frac{1 \cdot r}{12}$)/s; that is, the

Fig. 1 Apparatus of model test: **a** schematic diagram of model test; **b** actual indoor setup
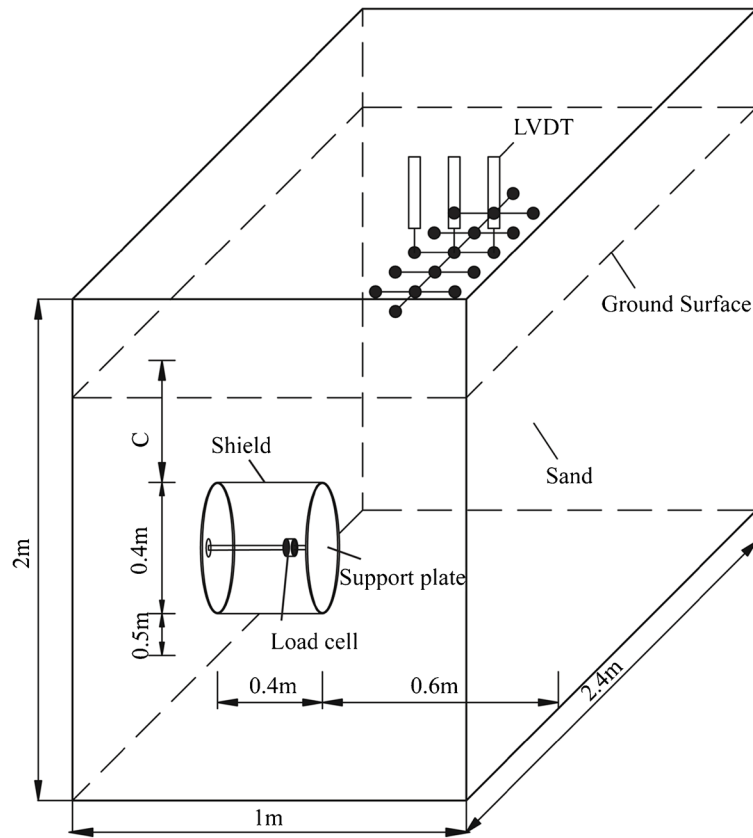

(a)
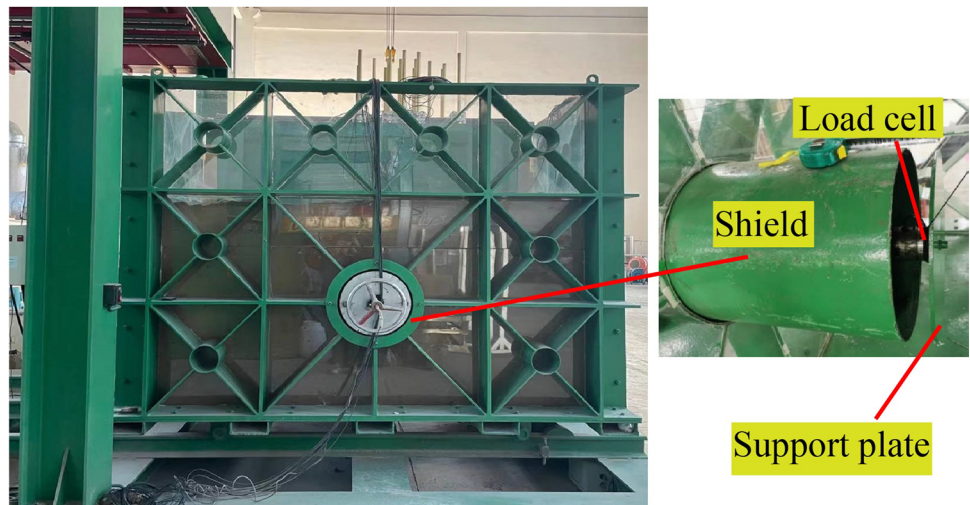
(b)

support plate moved backwards by 0.167 mm per 1/12 circle of screw rotation.

Characteristics of sands

In this paper, tests were performed with sands from Jinan. Nearly 80 tons of sands was oven-dried, and the grain size distribution of sands was determined by sieving method, which is shown in Fig. 4. In Fig. 4, the average grain size d_{50} is 1.7 mm; the nonuniformity coefficient C_u is 12.14, and coefficient curvature C_c is 0.11; the particle size distribution is uneven and its continuity is poor. Then, the sand was mixed with three different volumes of water evenly, and they were put into the chamber. In order to control the uniformity of relative density and degree of compaction, the uniformly mixing sand with same weight

Fig. 2 Locations of earth pressure cells: **a** front view; **b** side view

(a)

(b)
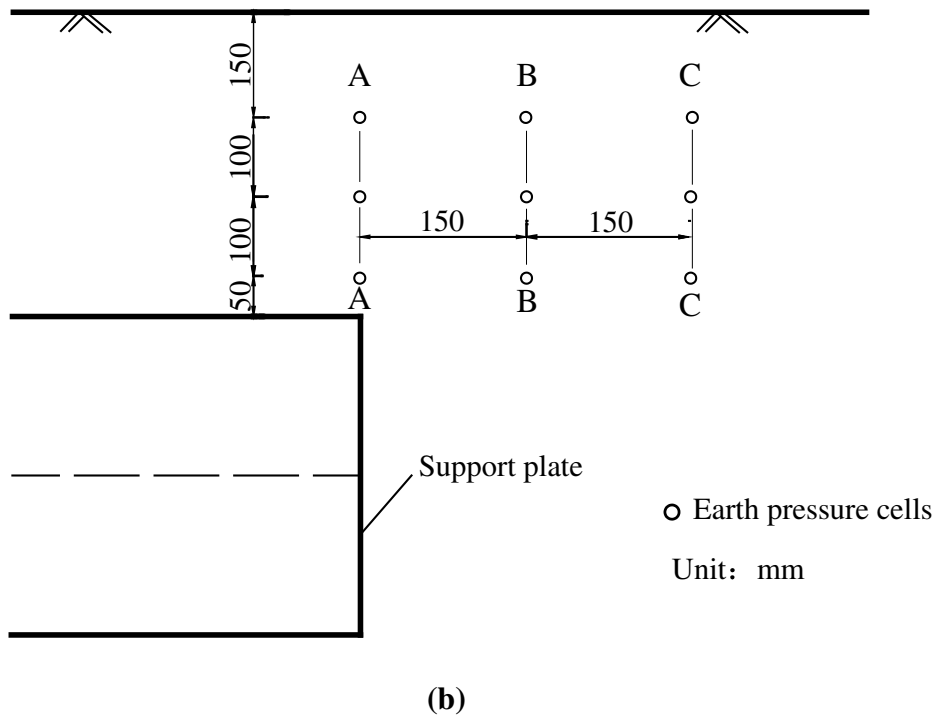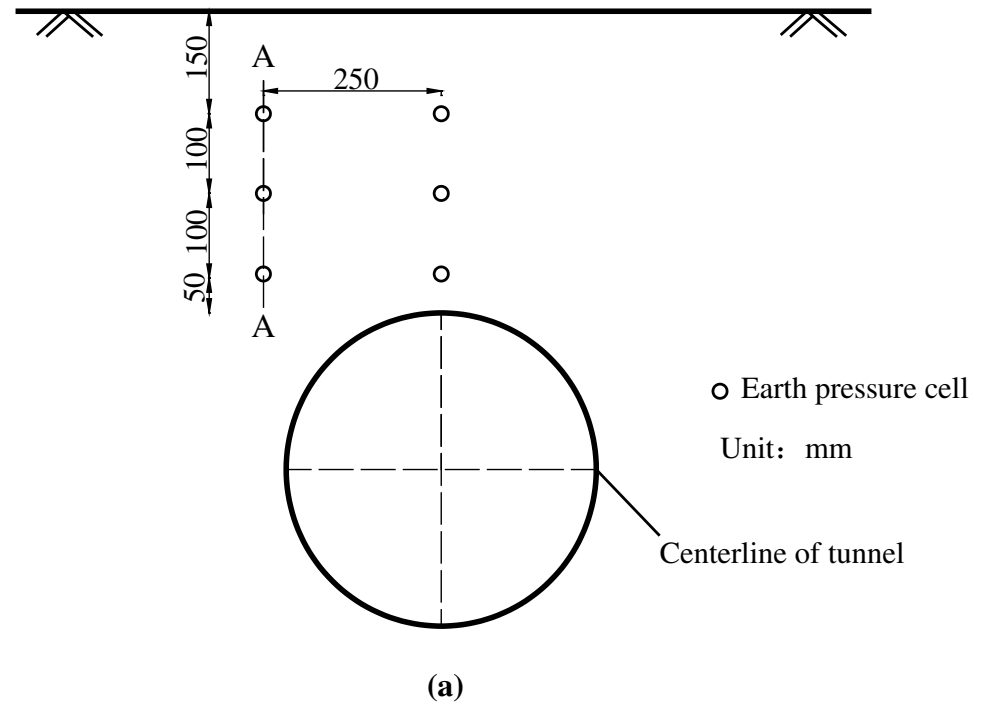
was put into the container layer by layer. Hand tamping was conducted with certain compaction energy to make each layer reach the height of 5 cm. Therefore, the uniformly mixing sand with same weight was compacted once at an interval of 5 cm, which is time-consuming but can ensure uniformity of relative density and degree of compaction to some extent. The same compaction method was also adopted by Liu et al. (2020a, b). Before each test, three sand samples from different locations were analyzed. Some relevant physical and mechanical parameters of sands were obtained by laboratory geotechnical test (see Table 1).
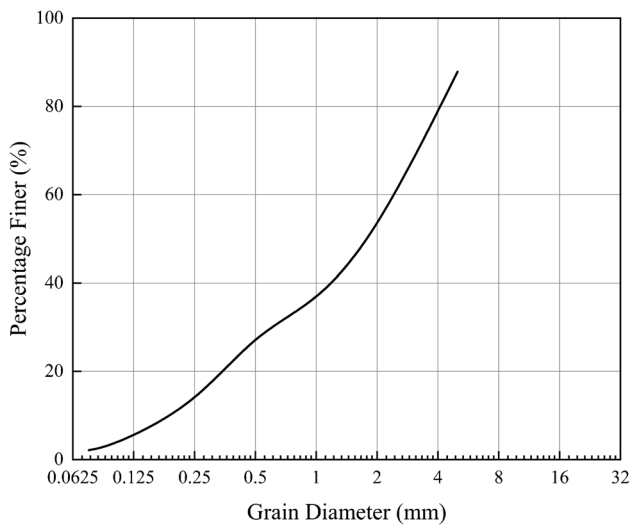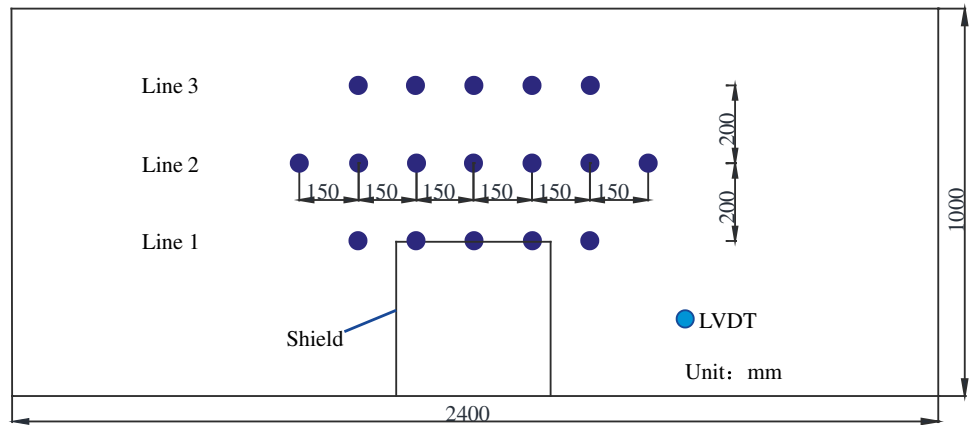
Fig. 3 Setup of LVDTs

Line 3

Line 2

150 150 150 150 150 150

Line 1

Shield

LVDT

Unit：mm

2400

Fig. 4 Particle size distribution curve of sand

of earth pressure cells is to input the calibration coefficient, which is obtained by sensor manufacturers from experiments, to data acquisition system (Labuz and Theroux 2005). Then, the average density and relative density were measured after the completion of filling.

(2) The ground surface was smoothed, and LVDTs were installed on the designed positions. The initial vertical earth pressures, support pressure, and surface settlement were recorded, then model tests started.

(3) The piston was rotated, and data obtained by LVDTs; earth pressure cells and load cells were recorded every 1 s.

(4) Instability occurred when there appeared steep drop in the load–displacement curve (Chen et al. 2013). The time to stop the model test can be adjusted according to test phenomenon, and data gained by the model tests should be recorded carefully.

Test procedure

The strain-controlled method was used by sequentially reducing the support pressure during tests, and the specific steps were as follows:

(1) The sand with uniform mixing and same weight was put into the chamber and compacted layer by layer. The earth pressure cells were put on the designed positions and calibrated prior to burial. The calibration method

Results and discussion

Face support pressure and face displacement

Variation of face support pressure

Figure 5 shows the curves of normalized face support pressure P/P_0 versus normalized face displacement δ/D from model tests for three moisture contents with $\omega = 1.43\%$,

Table 1 Physical and mechanical parameters of sands

Test number	Moisture content(%)	Density(g/cm^3)	Internal friction angle/°	Relative density	Degree of compaction (%)	Cohesion/kPa
1	1.43%	1.83	36.4	0.90	95	1.60
2	5.24%	1.71	36.1	0.64	86	2.33
3	9.3%	1.53	35.9	0.23	74	4.79
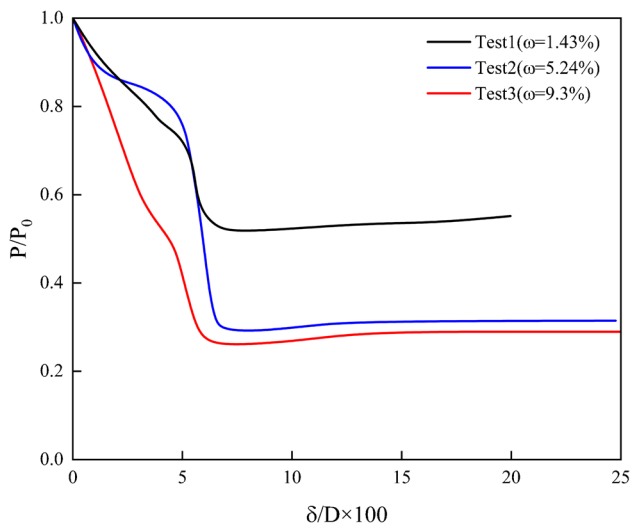
Fig. 5 Normalized load–displacement curves of three model tests

Fig. 6 Relationship between the limit support pressure and cover depth

5.24%, and 9.3%, where P and P_0 are the load and initial load acting on the tunnel face, respectively; δ is the face displacement.

In Fig. 5, the curves of normalized load–displacement from model tests with three moisture contents show the roughly same development trends, which can mainly be divided into four stages. The four stages can be described as:

(1) Stage 1: With the displacement of the support plate, the support pressure tends to decrease slowly, and the normalized load–displacement curve is approximately linear. There is a relative sliding trend between sands in front of the tunnel face and sands on both sides. In this stage, the shearing resistance of sands works and soil arching effect takes place.

(2) Stage 2: The support pressure decreases at a large rate, and it can reduce sharply to the limit support pressure, P_u, at the face displacement of about 0.06 D. In this stage, the sand in front of the tunnel face reaches the limit equilibrium state, the soil arching effect fully develops, and the load transferred to the sand on both sides gets the largest.

(3) Stage 3: The support pressure increases slightly to a stable value when the support plate continues to move backwards. A local collapse occurs with the limit shear strength reached. The original soil arching is damaged, and the new soil arching begins to form and propagate towards ground surface.

(4) Stage 4: The support pressure reaches a stable value, which does not change with the displacement of the support plate, and the global collapse occurs.

Figure 5 also shows that, different low moisture contents have little effect on the displacement that lead to the
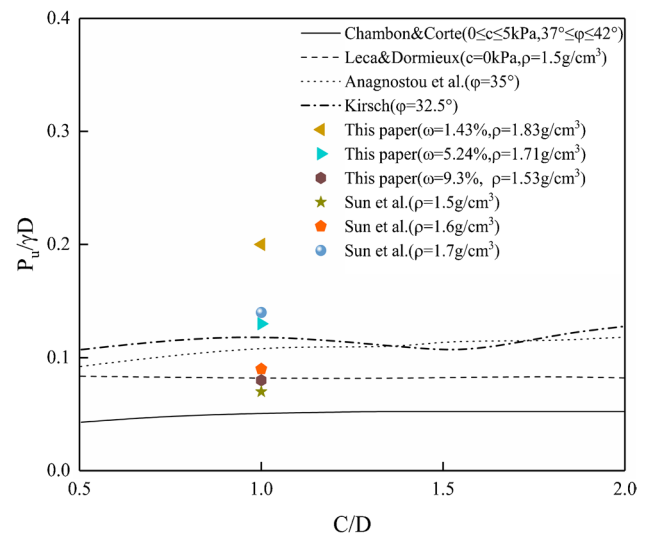
appearance of P_u with $C/D = 1$. The displacements are within the range of 24–30 mm. The reason is that, at the initial stage where soil arching begins to form, the range of failure zone is generally same in sands with different low moisture contents. However, P_u gradually decreases with the increase of moisture content, and the values of P/P_0 are 0.5, 0.3 and 0.26, respectively. The reason is that, there exists certain apparent cohesion in unsaturated sand due to the matrix suction, and the apparent cohesion increases with the increase of moisture content. It is obvious that sands with higher apparent cohesion show better shear resistance than dry sand. Therefore, with the increase of the moisture content, the adjoining stationary sands bear more pressure transferred from a yielding mass of sands, and the influence range of soil arching becomes larger; what is more, the sands are more stable, and the smaller limit support pressure P_u is required.

Comparison of limit support pressure

In Fig. 6, the dimensionless factor $P_u/\gamma D$ is introduced to compare with the existing results obtained by theoretical analysis and model tests.

Figure 6 shows that $P_u/\gamma D$ obtained from this paper with $\omega = 1.43\%$ is larger than that of existing researches. Furthermore, the increase of moisture content can lead to the decrease of sand density and the limit support pressure, which is in good agreement with the conclusion obtained by Sun et al. (2017), because various moisture contents lead to different sand properties such as sand density, internal friction angle, and apparent cohesion. In the case of a certain volume, the sand with lower moisture content has a greater self-weight due to its relatively high density, which can reach

the shearing resistance more easily. Thus, sands with lower moisture contents involve the small influence scope of soil arching effect. Similarly, it can be inferred that because the apparent properties of sands are similar, $P_u/\gamma D$ obtained by this paper is consistent with that obtained by Anagnostou and Kovári (1996) and Kirsch (2010) with $\omega = 5.24\%$; $P_u/\gamma D$ is close to that calculated by Leca and Dormieux (1990) with $\omega = 9.3\%$. In addition, in this paper, $P_u/\gamma D$ decreases with the increasing moisture content with $C/D = 1$, but it presents a slower reduce trend. When the moisture content of sand reaches a high constant, the apparent cohesion begins to decrease. Thus, it can be inferred that the limit support pressure will increase again. $P_u/\gamma D$ obtained in this paper coincides with that obtained by model tests and calculated by theoretical analysis, which proves the effectiveness of this model test.

Analysis of ground settlement

Variation of ground settlement

As shown in Fig. 7, the ground settlement laws of settlement center in sand with different low moisture contents are different. The ground settlement of Test 2 can be divided into four stages. The stages and possible reasons can be described as:

(1) Stage 1: There is no ground subsidence with the displacement of the support plate. In this stage, the evolution of soil arching begins but the arch zone does not propagate to ground surface;

(2) Stage 2: The ground surface subsides at a slow rate. In this stage, the arch zone continues to propagate towards the ground surface and reaches the surface;
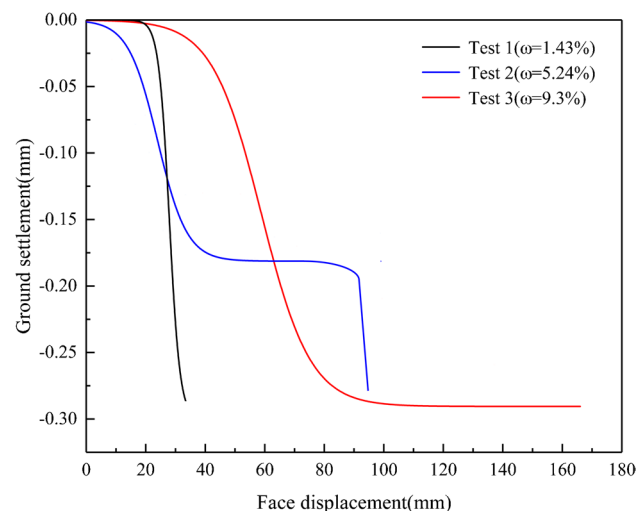
(3) Stage 3: With the increase of the face displacement, there is no obvious ground subsidence. The residual soil arching forms and starts working, and the internal sand is aggregated into blocks;

(4) Stage 4: The settlements increase steeply. In this stage, a global collapse occurs, and the soil arching is destroyed, which make ground surface collapse suddenly.

It should be noted that for Test 1, there is no Stage 3 and Stage 4 in terms of ground settlement. The ground surface collapses suddenly with the face displacement of 26 mm. At this time, the soil arching is completely destroyed and the sand is in a state of global collapse; for Test 3, there is no Stage 4 compared with Test 2. With the increase of face displacement, the settlement basically shows a linear growth, and a constant value is reached after the displacement of 100 mm. Furthermore, the soil arching effect is obvious, and the sand in front of the tunnel face is not in a state of global collapse, that is to say, the failure zone does not propagate to the ground surface. This shows to some extent that the increase of moisture content in sand leads to the increasing apparent cohesion and better self-stability of sand.

Surface settlement trough

Based on a considerable number of field observations, Peck (1969) concluded that the transverse settlement trough can be expressed as follows:

$$S = S_{\max} e^{-\frac{x^2}{2i^2}} \tag{1}$$

where S and $S_{\max}$ are the settlement and maximum settlement, respectively; x is the distance from one point on the ground face to the centerline; and i is the distance from the point of inflection on the settlement trough to tunnel centerline.

O'Reilly and New (1982) analyzed the monitoring data of tunnels in London, and they concluded that the relationship between the point of inflection i and the depth of tunnel centerline Z_0 can be expressed as follows:

$$i = K Z_0 \tag{2}$$

where K is a parameter of width coefficient of settlement trough, which depends not on the tunnel size and construction method but the soil nature. Existing field data (Mair et al. 1993) indicate that K varies between 0.2 and 0.45 for sands and gravels.

The settlement trough is drawn by the settlement value of Line 2 before the occurrence of global collapse, and the fitting of Gaussian distribution is carried out (see Fig. 8).

Figure 8 shows that settlement values corresponding to the three moisture contents can fitting well with Gaussian
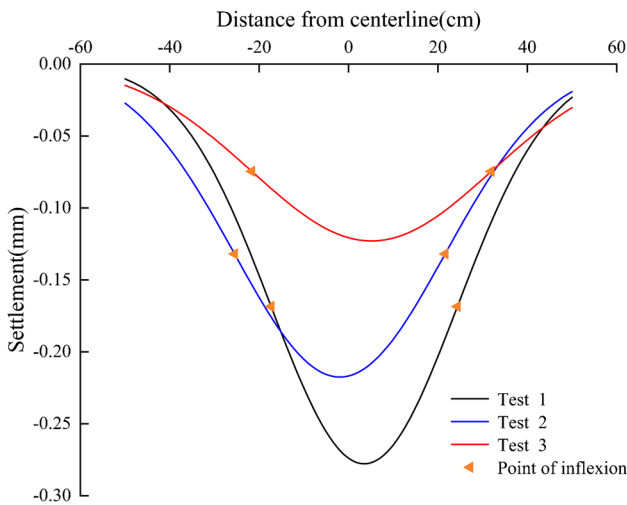
Fig. 7 Relationship between ground settlement and face displacement

Fig. 8 Curves of Gaussian distribution fitting of line 2

distribution curve for Line 2, which effectively proves the rationality of Peck formula. As shown in Fig. 9a, the values of i obtained from Tests 1, 2, and 3 are 20.84 cm, 23.55 cm, and 26.79 cm, respectively. Thus, with the increasing moisture content, the value of i is larger; that is, the expansion range of settlement trough is larger, and settlement trough is "shallow and wide"; on the contrary, the settlement trough is "narrow and deep." This also reflects, to some extent, the soil arching has a greater effect on reducing the settlement due to the decreasing support pressure with the increase of moisture content.

By using Eq. (2), the values of K with three different moisture contents can be calculated as 0.35, 0.39, and 0.45, respectively. They are all between 0.2 and 0.45, which coincide with the results obtained from existing field data (Mair et al. 1993). Therefore, the higher the moisture content is, the larger the expansion range of settlement trough is. As shown in Fig. 9b, the relationship curve between K and moisture content is drawn. In addition, in the range of moisture content from 1.34 to 9.3%, the fitting relationship between them is

$$K = 0.012\omega + 0.329 \tag{3}$$

This formula can be used to approximately predict the value of K for shallow tunnels in sandy ground with moisture content from 1.34 to 9.3%. However, it is worth noting that this formula cannot predict the value of K when the moisture content exceeds 9.3% due to the limitation of the number of tests.

Analysis of distribution of earth pressure

Distribution of earth pressure

According to Chen et al. (2013), the vertical stress concentration ratio, λ, is defined as $\lambda = \sigma_v / \sigma_{v0}$ to observe the stress
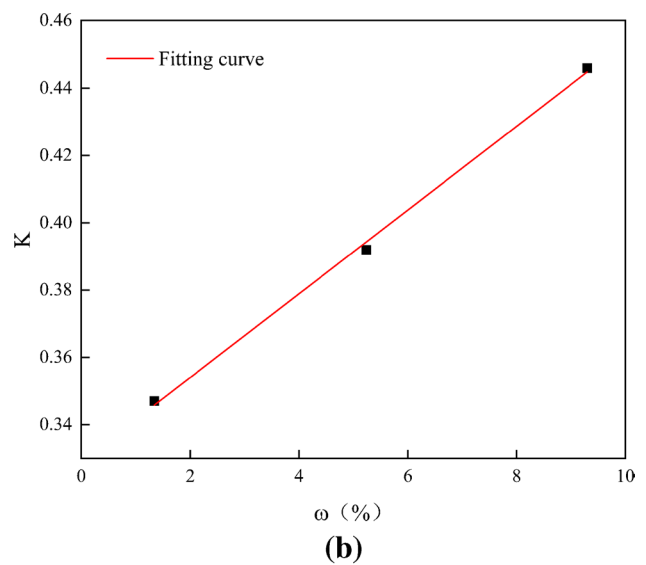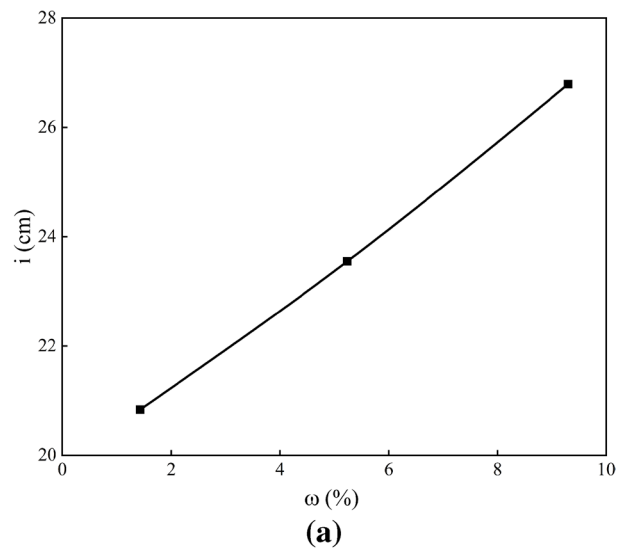

Fig. 9 Influence of moisture content on related parameters of settlement trough: **a** relationship between i and ω; **b** relationship between K and ω

distribution and the evolution of soil arching in front of tunnel face, where σ_v is the final vertical earth pressure and σ_{v0} is the initial vertical earth pressure. Distributions of earth pressure with the three different moisture contents are shown in Fig. 10.

As shown in Fig. 10, when $\omega = 9.3\%$, λ at the position of 0.5 D in front of tunnel face gradually increases from bottom to top and is close to 1.0 at the position of 0.15 m away from the ground surface. At this time, earth pressure in the yielding mass of sand is released, and the loose failure zone appears, which lead to the decrease of vertical earth pressure. In addition, λ increases slightly in the adjoining stationary part of sand, indicating that the soil arching is formed and not destroyed. It can be inferred that the arch
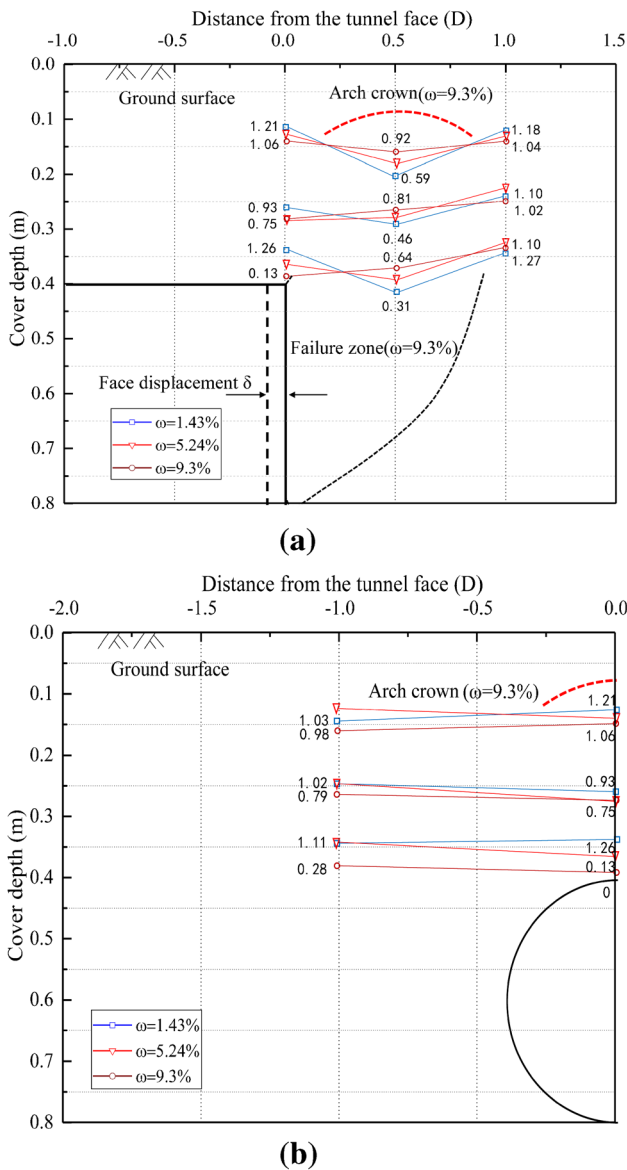
Fig. 10 Distribution of vertical earth pressure: **a** longitudinal profile; **b** cross profile

Analysis of soil arching effect

With the displacement of the tunnel face, the face support pressure decreases, and the vertical earth pressure decreases rapidly. Furthermore, earth pressure is transferred from the yielding sand onto adjoining stationary parts, and the soil arching takes place. Then, as the tunnel face continues to retreat, the soil arching effect develops to the maximum, and the corresponding support pressure currently is the limit support pressure. Next, arch zone propagates upwards the ground surface, and the support pressure increases slightly; meanwhile, the ground surface begins to subside at a slow rate. When the ground settlement reaches a certain value, the small displacement of tunnel face will lead to large ground settlement for sands with lower moisture content. Finally, the arch zone propagates to the ground surface, and global collapse occurs. In this stage, the soil arching will be destroyed, and the support pressure tends to be a constant value. However, due to the greater apparent cohesion in sand with higher moisture content, the soil arching is not destroyed at last, and the soil arching is significant in maintaining the face stability. It was also found that the cavity was formed with $\omega = 9.3\%$. The evolution of soil arching with different moisture contents are illustrated in Fig. 11.

Actual tunnel face failure morphology of model tests in sand with different moisture contents are shown in Fig. 12. It is obvious that, in Tests 1 and 2, the failure zone propagates to the surface, and global collapse occurs, which means the soil arching is destroyed eventually. Compared with the failure morphology in Test 1, failure zone in Test 2 is larger due to the smaller internal friction angle, and the obvious collapse phenomenon occurs. The reason is that higher moisture content corresponds to more significant apparent cohesion, which means that the limit support pressure required to maintain face stability of sand is smaller. During model tests, the strain-controlled method is used to reduce the support pressure by making the support plate backward. And for Test 1, it takes a much shorter retreat to reach the limit support pressure. Therefore, since the backward space is much smaller than the surface settlement space when the global collapse occurs, there is no obvious collapse phenomenon like Test 2. As shown in Fig. 12c, there seems no obvious settlement and failure in Test 3. When $\omega = 9.3\%$, the soil arching effect still exists, and the sand has reached the state of self-stability. Therefore, the higher moisture content corresponds to greater apparent cohesion, smaller internal friction angle, and more significant soil arching, and soil arching play an important role in maintaining the face stability.
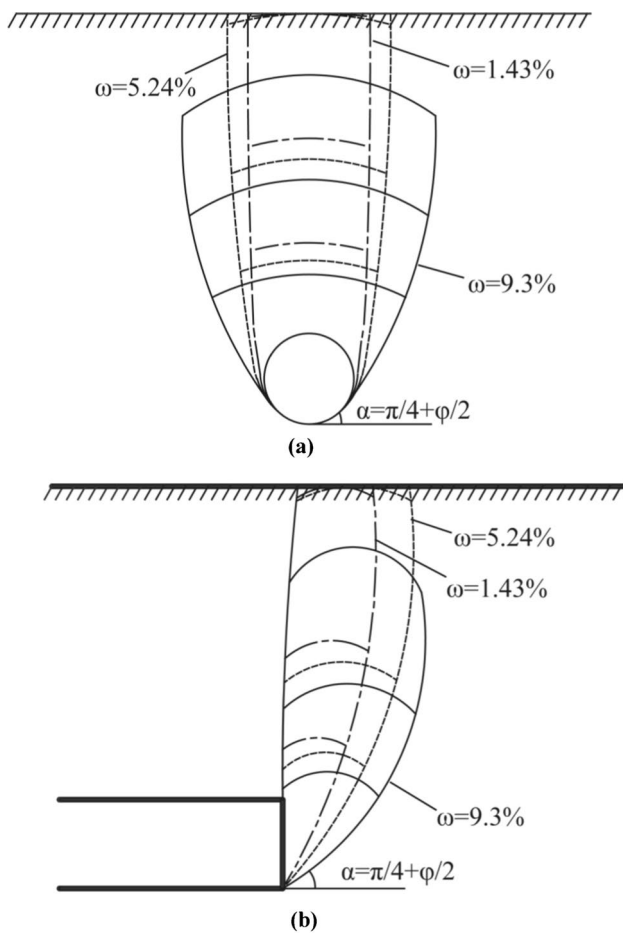
crown is approximately 0.2–0.25 D away from the ground surface. With the decrease of the moisture content, λ at the position of 0.5 D in front of tunnel face is always less than 1.0; the reason is that the arch zone has propagated to ground surface and the soil arching effect disappears at this time, which make the sand in a state of global collapse. Figure 10 also shows that with the increase of moisture content, the area where λ changes become bigger; that is, the expansion range of the failure area is larger. This is consistent with the conclusions drawn from the previous context.

Fig. 11 Diagram of evolution of soil arching: **a** cross-section; **b** longitudinal section

Failure mechanisms

Relative theories

Upper bound theorem of limit analysis

This theorem can be described as follows: the load corresponding to the kinematic allowable deformation field is the upper bound of the real load, which corresponds to the motion state of the research object. Chen (1975) held that in any kinematically admissible deformation field, the load determined by the equation of virtual work is always larger than the actual failure load, and the equation is given as follows:

$$\int_S F_i v_i^* dS + \int_A \gamma_i v_i^* dA = \int_A \sigma_{ij} \varepsilon_{ij}^* dA + \int_{S_D} \left(\tau - \sigma_n \tan \phi\right) \Delta v_t^* dS \tag{4}$$

where A is the plastic zone; S is the plane of rupture; τ and σ_n are shear stress and normal stress, respectively; σ_{ij} is the stress, F_i is collapse load, and γ_i is the unit weight of soil.

In Eq. (4), F_i is generally considered as the ultimate load to make the system collapse, but there are also some special cases. In this paper, the vertical support pressure applied to the surrounding rock is used to prevent the tunnel face from being damaged, which is generally less than the actual failure load.

Stability ratio N

The stability ratio N was introduced by Broms and Bennermark (1967), which can be expressed by

$$N = \frac{\sigma_S - \sigma_T + \gamma(C + D/2)}{c_u} \tag{5}$$

where σ_S is uniform pressure acts on ground surface; σ_T is the pressure acts on the surrounding rock; and c_u is undrained shear strength.

On this basis, Davis et al. (1980) applied the criteria for judging the face stability in cohesive soil layers: if N is higher than 6, the shallow tunnel is in an unstable state, and if N is less than 6, the shallow tunnel will be stable.

Construction of failure mechanisms

Basic assumptions

There are many factors that affect the support pressure of shield tunnel. In order to simplify the construction of failure mechanisms, the following assumptions are made:

(1) The calculation in this paper can be regarded as a plane strain problem.
(2) The circular tunnel is simplified into a square tunnel, and the width of the square tunnel is equal to D.
(3) The pressure acts on the top, sides, and bottom of the surrounding rock is uniform.
(4) The change of soil volume in this process is ignored.

Failure mechanisms

Atkinson and Potts (1977) suggested that failure mechanisms should be determined by analyzing the variation of earth pressure and ground settlement and observing the actual failure shape during model tests. Furthermore, Chen et al. (2013) proposed that the excavation of tunnels will induce redistribution of earth stress, and the P_u is far less than the initial support pressure due to the soil arching. Thus, soil arching is a key factor to be considered when constructing failure mechanisms. However, the soil arching effect is often

Fig. 12 Failure morphology with different moisture contents: **a** Test 1 ($\omega=1.43\%$); **b** Test 2 ($\omega=5.24\%$); **c** Test 3 ($\omega=9.3\%$)

(a)

(b)

(c)
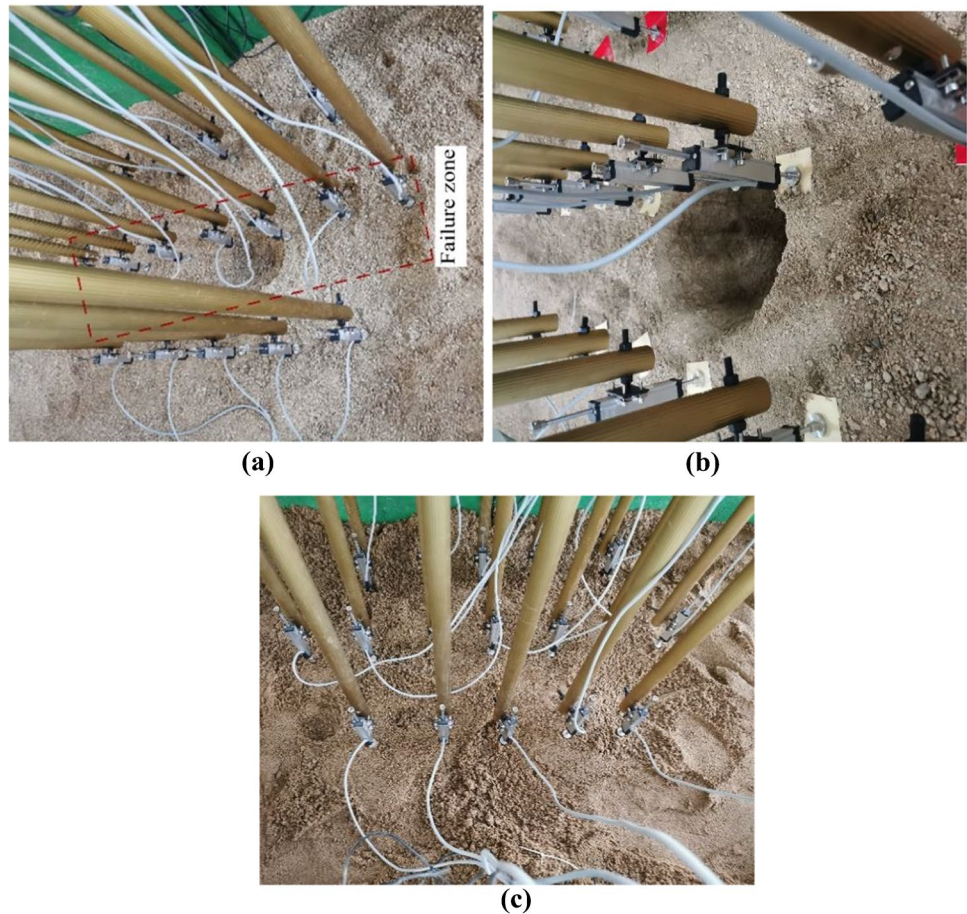
ignored when calculating the limit support pressure. Therefore, combined with the actual range of ground settlement and distribution of vertical earth pressure, considering the influence of soil arching effect on tunnel face stability, the failure mechanisms under three different moisture contents ($\omega=1.43\%$, 5.24%, and 9.3%) were constructed, as shown in Fig. 13.

The model test results with $\omega = 1.43\%$ show that the settlement trough is "narrow and deep," and the failure zone propagates to the surface. Moreover, the value of P_u/P_0 is about 0.5, which means the support pressure does not reduce too much with the displacement of tunnel face. And soil arching is not developed well and eventually destroyed. The internal friction angle, φ, is larger than that in sand with higher moisture content. Therefore, the top failure model can be adopted, as shown in Fig. 13a. For sands with $\omega = 5.24\%$, both the width of settlement trough i and the failure zone become larger, and the arch zone reaches the surface. Furthermore, P_u/P_0 is reduced to 0.3, the soil arching effect is further developed, and failure mechanism 2 can be constructed as shown in Fig. 13b; for sands with $\omega = 9.3\%$, the settlement trough is "wide and shallow," and the arch zone does not reach the surface. P_u/P_0 is reduced to 0.26, and the soil arching effect is obvious. Considering the influence of

soil arching effect on face stability and the range of ground settlement obtained from model tests, failure mechanism 3 can be constructed as shown in Fig. 13c. As shown in Fig. 13c, arch EF can be described as a parabola in the form of $y = x(1 - x/B)\tan\alpha$ with B being the arch width, α the inclination angle at the foot of the arch with $\alpha = 45° + \frac{\varphi}{2}$, and H the height of the arch with $H = B\tan(\alpha/4)$ (Guo and Zhou 2013).

In this paper, it is assumed that the angle between the slip surface and the velocity on it is equal to half of the internal friction angle of the sand, that is, $\varphi' = \frac{\varphi}{2}$; and the angle between the rupture surface and the horizontal line is equal to α with $\alpha = 45° + \frac{\varphi}{2}$. Taking vector closure condition into consideration, the velocity field corresponding to failure mechanisms 2 and 3 can be obtained, as shown in Fig. 14.

Calculation of limit support pressure

Due to the limited space, only the calculation process of failure mechanism 2 is illustrated in detail. Failure mechanism 2 is an axisymmetric structure, so it can be calculated by semi-structure.
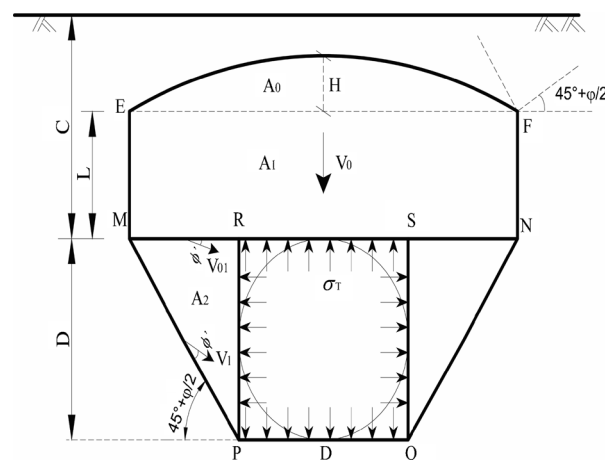
(1) Calculation of kinematically admissible velocity field

Fig. 13 Failure mechanisms with different moisture contents: **a** failure mechanism 1 ($\omega = 1.43\%$); **b** failure mechanism 2 ($\omega = 5.24\%$); **c** failure mechanism 3 ($\omega = 9.3\%$)
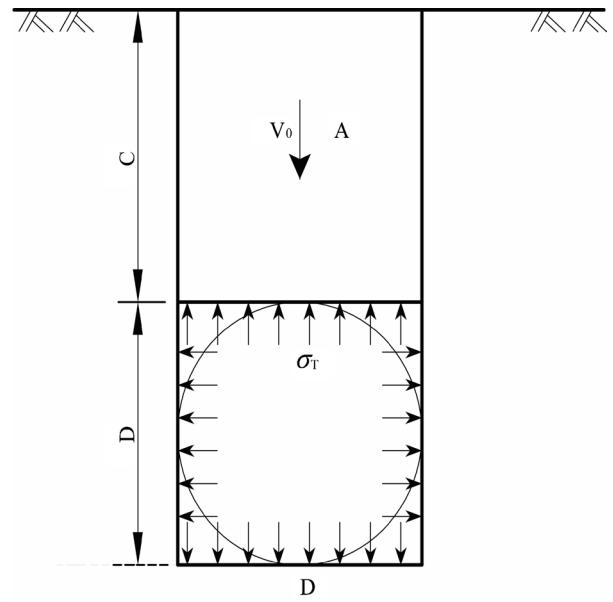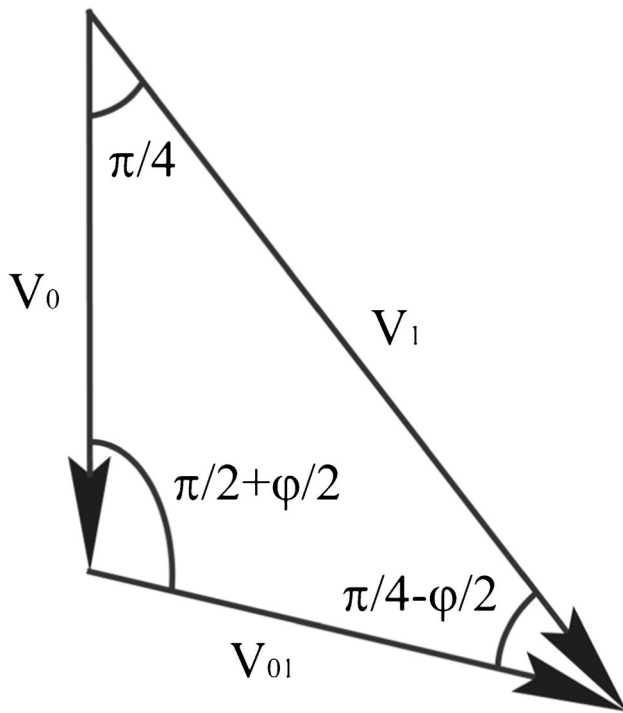

(a)
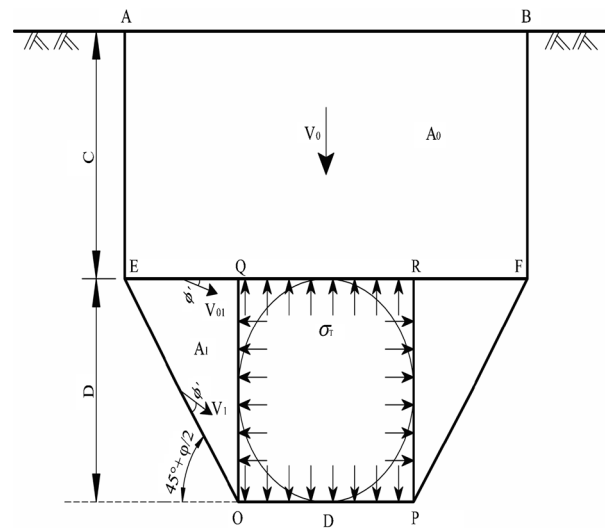
(b)

(c)

Fig. 14 Velocity field corresponding to failure mechanisms 2 and 3

When using the rigid block theory, the vector closure condition should be satisfied for the velocity vectors. According to the velocity field, the following equivalent relations can be obtained:

$$v_1 = \frac{\sin(\frac{\pi}{2} + \frac{\varphi}{2})}{\sin(\frac{\pi}{4} - \frac{\varphi}{2})} v_0 \tag{6}$$

$$v_{01} = \frac{\sin \frac{\pi}{4}}{\sin(\frac{\pi}{4} - \frac{\varphi}{2})} v_0 \tag{7}$$

(2) Area of rigid sliding-block and length of discontinuous line

According to the geometric relationship in Fig. 13b, the area of rigid sliding-block and length of discontinuous line can be obtained as:

$$EQ = \frac{D}{\tan \alpha}; \ EO = \frac{D}{\sin \alpha}; \ EF = D + \frac{2D}{\tan \alpha};$$

$$A_0 = \frac{1}{2} \cdot C \cdot EF; \ A_1 = \frac{1}{2} \cdot D \cdot EQ$$

(3) Calculation of σ_T and N

The power of the sand weight is written:

$$P_\gamma = \gamma \frac{C \cdot EF}{2} v_0 + \gamma \frac{EQ \cdot D}{2} v_1 \cos \frac{\pi}{4}$$
$$= \gamma D^2 v_0 \left[\frac{C}{D} f(\varphi) + f_1(\varphi) \right] \tag{8}$$

where $f(\varphi) = \frac{2 + \tan \alpha}{2 \tan \alpha}; f_1(\varphi) = \frac{\sin(\frac{\pi}{2} + \frac{\varphi}{2}) \cos \frac{\pi}{4}}{2 \tan \alpha \sin(\frac{\pi}{4} - \frac{\varphi}{2})}.$

The power of support pressure on the top and side of the tunnel is written:

$$P_T = -\sigma_T \frac{D}{2} v_0 - \sigma_T D v_1 \cos \frac{\pi}{4} = -\sigma_T D v_0 f_2(\varphi) \tag{9}$$

where $f_2(\varphi) = \frac{1}{2} + \frac{\sin\left(\frac{\pi}{2} + \frac{\varphi}{2}\right) \cos \frac{\pi}{4}}{\sin\left(\frac{\pi}{4} - \frac{\varphi}{2}\right)}.$

The dissipation power can be written:

$$P_V = c_u \cdot AE \cdot v_0 + c_u \cdot EO \cdot v_1 \cos \varphi + c_u \cdot EQ \cdot v_{01} \cos \varphi$$
$$= c_u D v_0 \left[\frac{C}{D} + f_3(\varphi) \right] \tag{10}$$

where $f_3(\varphi) = \frac{\sin\left(\frac{\pi}{2} + \frac{\varphi}{2}\right) \cos \frac{\varphi}{2}}{\sin \alpha \sin\left(\frac{\pi}{4} - \frac{\varphi}{2}\right)} + \frac{\sin \frac{\pi}{4} \cos \frac{\varphi}{2}}{\tan \alpha \sin\left(\frac{\pi}{4} - \frac{\varphi}{2}\right)}.$

According to the equation of virtual work, the power of external forces is equal to the dissipation power, which can be expressed by

$$P_\gamma + P_T = P_V \tag{11}$$

Finally, the limit support pressure σ_T and stability ratio N are obtained as follows:

$$\sigma_T = \frac{P_\gamma - P_V}{D v_0 f_2(\varphi)} \tag{12}$$

$$N = \frac{\sigma_S - \sigma_T + \gamma(C + D/2)}{C_u} = \frac{\gamma D [f_2(\varphi) - 2f_1(\varphi)]}{C_u \cdot 2f_2(\varphi)} + \frac{C}{D f_2(\varphi)} + \frac{\gamma C [f_2(\varphi) - f(\varphi)]}{C_u f_2(\varphi)} + \frac{f_3(\varphi)}{f_2(\varphi)} \tag{13}$$

Comparison with existing research

In order to verify the rationality of failure mechanisms presented in our study, the σ_T and N obtained by the three model tests are compared with those of the theoretical solutions, as shown in Figs. 15 and 16.

In Fig. 15, the σ_T of failure mechanisms 1 and 2 are between the upper- and lower-bound solutions of Sloan and Assadi (1993) when $\rho = 0.25$, and are close to the upper-bound solutions obtained by Osman et al. (2006) when $\rho = 0.25$, where ρ is the rate of change of shear strength with depth. This shows that, due to the uneven distribution of moisture content in sand, failure mechanisms 1 and 2 are more suitable for sandy ground with ρ being approximately 0.25 in practical engineering. The limit support pressure of failure mechanism 3 is larger than upper-bound solutions
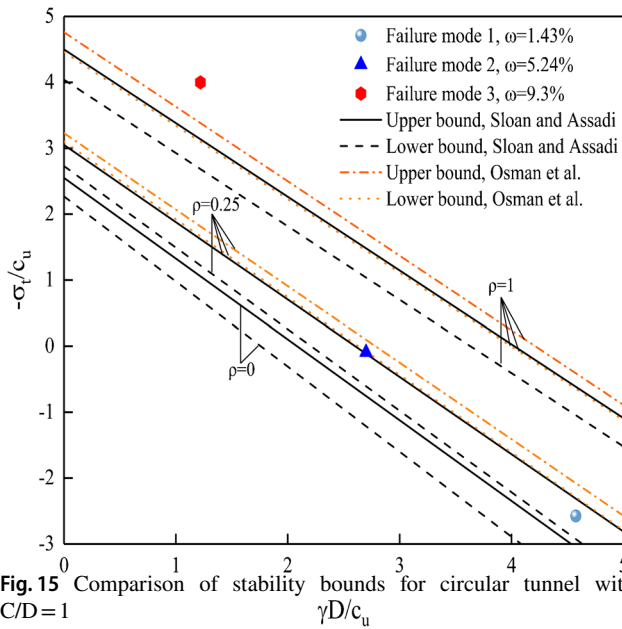
Fig. 15 Comparison of stability bounds for circular tunnel with $C/D = 1$
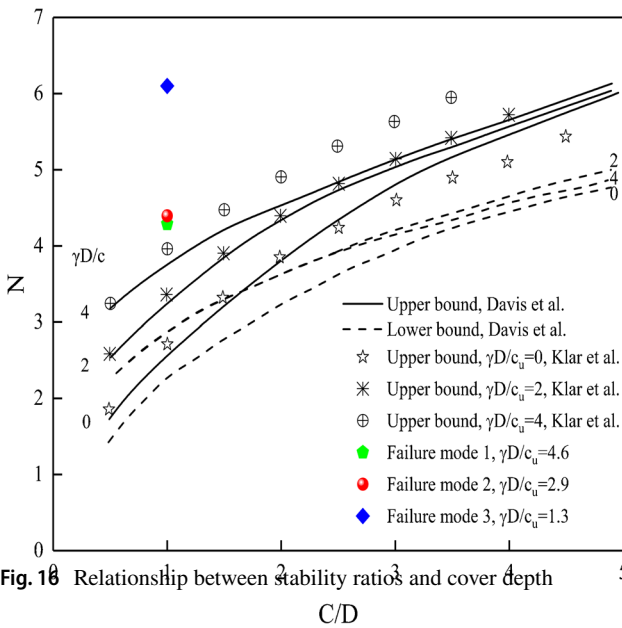

Fig. 16 Relationship between stability ratios and cover depth

when $\rho = 1$. The reason is that the mechanisms presented by Sloan and Assadi (1993) and Osman et al. (2006) do not take the soil arching effect into consideration. However, the existence of soil arching greatly reduces the value of σ_T. Therefore, the existing researches overestimate the σ_T.

Figure 16 shows the relationship between N and C/D. The solutions of failure mechanism 1 and 2 are all less than 6 with $C/D = 1$. In addition, the stability ratio N of failure mechanism 1 is close to the upper-bound solutions obtained by Davis et al. (1980) and Klar et al. (2010), but N of failure mechanism 2 is slightly larger. The possible reason is the circular tunnel is equivalent to a square tunnel when the limit support pressure is calculated by failure mechanisms

presented in this paper, and the square tunnel is prone to stress concentration, which makes the structure unsafe and the stability coefficient N larger. The stability ratio N of failure mechanism 3 is equal to 6.1, which is quite different from the upper-bound solutions presented by Davis et al. (1980) and Klar et al. (2010). The reason is that when constructing failure mechanism 3, the influence of soil arching effect is considered. The existence of soil arching prevents the failure from propagating to the surface. Thus, the limit support pressure is smaller, and the stability ratio N will be larger.

In order to analyze the influence of different low moisture contents on the face stability in sand more intuitively, the
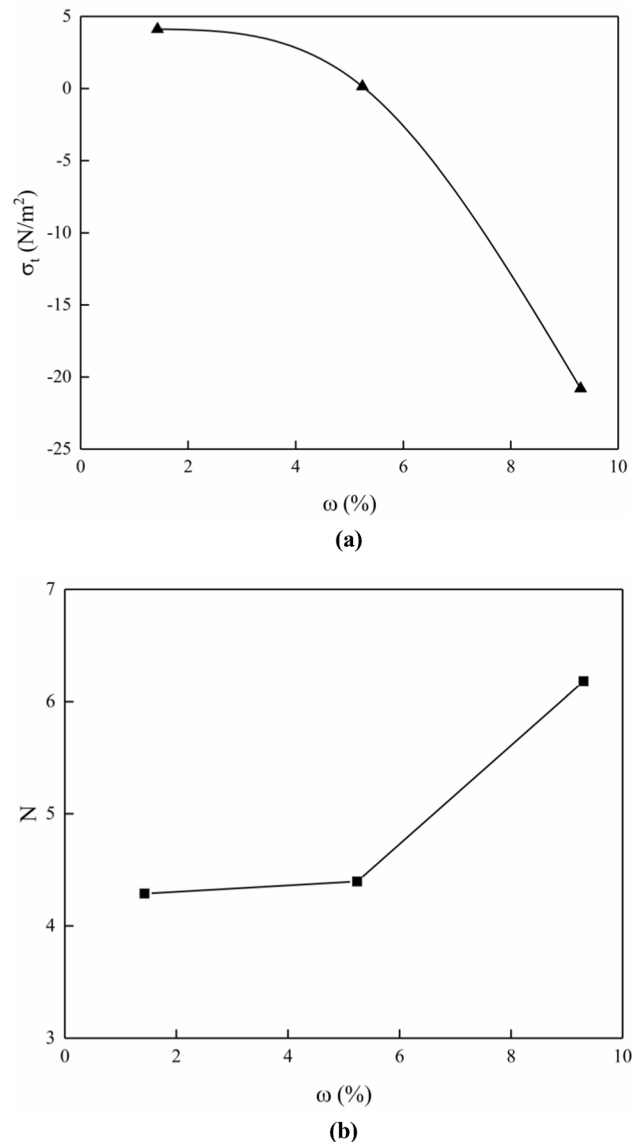

(a)

(b)

Fig. 17 Influence of different low moisture contents on face stability: **a** relationship between σ_t and moisture content; **b** relationship between N and moisture content

relationship between stability solutions and moisture content is drawn (see Fig. 17).

Figure 17 shows that, with the increase of the moisture content, σ_T decreases and stability ratio N becomes larger. When $\omega = 9.3\%$, the limit support force is negative; that is to say, the tunnel face can be stable without support. Owing to the increase of moisture content, the apparent cohesion of sand increases, and soil arching effect plays a more significant role in keeping the sand stable, which also makes the limit support pressure far less than the initial value. It can also be inferred that, when the soil arching effect is considered, the stability ratio N of shield tunnel in sand with low moisture content is higher than the critical value of N in cohesive soils proposed by Davis et al. (1980)

Conclusions

In order to obtain the variation laws of face support pressure, ground settlement, and vertical earth pressure in unsaturated sand, large-scale geo-mechanical model tests of shield tunnels in sands with different low moisture contents ($\omega = 1.43\%$, 5.24%, and 9.3%) were undertaken. The failure mechanisms under three different moisture contents ($\omega = 1.43\%$, 5.24%, and 9.3%) were constructed considering arching effect. Compared with the existing researches, the proposed failure mechanisms are more suitable to practical projects. The main conclusions are as follows:

(1) The moisture content has a significant influence on failure mechanisms, limit support pressure, and the evolution of soil arching effect when $C/D = 1$. The ratios of P_u/P_0 gradually reduce with the increasing moisture content, which are 0.5 ($\omega = 1.43\%$), 0.3 ($\omega = 5.24\%$), and 0.26 ($\omega = 9.3\%$), respectively. This shows within a certain range of moisture content, the soil arching effect is more significant in maintaining the face stability with the moisture content being higher, and the existence of soil arching makes limit face support pressure much smaller than the initial support pressure.

(2) The curves of ground settlement corresponding to sands with different low moisture contents are various. With the increasing moisture content, the settlement trough is wider, and the settlement value at the center of settlement trough is smaller. Within a certain range of moisture content, there is a linear relationship between the width coefficient of settlement trough and the moisture content.

(3) Higher moisture contents lead to the larger area where vertical stress concentration ratio, λ, changes, which means the soil arching has a larger influence area. When the moisture content is relatively low, the fail-

ure zone propagates to the surface, and the soil arching effect disappears; when $\omega = 9.3\%$, the soil arching is not destroyed, and the distance from arch crown to ground surface is about $0.2 \sim 0.25$ D.

(4) Stability solutions calculated by failure mechanisms 1 and 2 are close to those obtained by existing researches. For failure mechanisms 3, the σ_t is smaller than that obtained by existing methods, and the stability ratio is larger than that of existing researches. Because the construction of failure mechanisms 3 involves the soil arching effect. It can also be inferred that, when considering the soil arching effect, the stability ratio N of shield tunnel in sand with low moisture content is higher than the critical value of N in cohesive soils proposed by Davis et al. (1980).

Author contribution All authors contributed to the manuscript. The tests were carried out by Zhongrong Wang, Wantao Ding, and Rui Chen; the data analysis were performed by Zhongrong Wang, Xinghang Huang, and Keqi Liu. The first draft of the manuscript was written by Zhongrong Wang, and all authors commented on previous versions of the manuscript. All authors read and approved the final manuscript.

Declarations

References

Alagha ASN, Chapman DN (2019) Numerical modelling of tunnel face stability in homogeneous and layered soft ground. Tunn Undergr Space Technol 94(11):1–14

Anagnostou G, Kovári K (1996) Face stability conditions with earth-pressure-balanced shields. Tunn Undergr Space Technol 11(2):165–173

Atkinson JH, Potts DM (1977) Stability of a shallow circular tunnel in cohesionlesss oil. Geótechnique 27(2):203–215

Broms BB, Bennermark H (1967) Stability of vertical openings in clays. J Soil Mech Found Div 93(1):71–94

Chambon P, Corté J (1994) Shallow tunnels in cohesionless soil: stability of tunnel face. J Geotech Eng 120(7):1148–1165

Chen WF (1975) Limit analysis and soil plasticity. Elsevier, Amsterdam

Chen RP, Tang LJ, Ling DS, Chen YM (2011) Face stability analysis of shallow shield tunnels in dry sandy ground using the discrete element method. Comput Geotech 38(2):187–195

Chen RP, Li J, Kong LG, Tang LJ (2013) Experimental study on face instability of shield tunnel in sand. Tunn Undergr Space Technol 33(1):12–21

Chen RP, Yin XS, Tang LJ, Chen YM (2018) Centrifugal model tests on face failure of earth pressure balance shield induced by steady state seepage in saturated sandy silt ground. Tunn Undergr Space Technol 81:315–325

Davis EH, Gunn MJ, Mair RJ, Seneviratne HN (1980) The stability of shallow tunnels and underground opening in cohesive material. Géotechnique 30(4):397–416

Ding WT, Li SC, Liu KQ, Zhu J et al (2018) Using a pressurized shield to increase face stability of circular tunnels in purely cohesive soil. Int J Geomech 18(9):1–11

Ding WT, Liu KQ, Shi PH, Li MJ, Hou ML (2019) Face stability analysis of shallow circular tunnels driven by a pressurized shield in purely cohesive soils under undrained conditions. Comput Geotech 107:110–127

Ding WT, Wang H, Liu KQ, Hou ML, Chen R (2021) Stability evaluation model of a tunnel face excavated by the benching method in a soft silty clay layer. Int J Geomech 4(21):04021022

Guo PJ, Zhou SH (2013) Arch in granular materials as a free surface problem. Int J Numer Anal Methods Geomech 37(9):1048–1065

Idinger G, Aklik P, Wu W, Borja RI (2011) Centrifuge model test on the face stability of shallow tunnel. Acta Geotech 6(4):105–117

Kirsch A (2010) Experimental investigation of the face stability of shallow tunnels in sand. Acta Geotech 5(1):43–62

Klar A, Osman AS, Bolton M (2010) 2D and 3D upper bound solutions for tunnel excavation using "elastic" flow fields. Int J Numer Anal Methods Geomech 31(12):1367–1374

Labuz JF, Theroux B (2005) Laboratory Calibration of Earth Pressure Cells. Geotech Test J 28(2):188–196

Lavasan AA, Zhao C, Barciaga T, Schaufler A, Steeb H, Schanz T (2018) Numerical investigation of tunneling in saturated soil: the role of construction and operation periods. Acta Geotech 13(3):671–691

Leca E, Dormieux L (1990) Upper and lower bound solutions for the face stability of shallow circular tunnels in frictional material. Géotechnique 40(4):581–606

Li W, Zhang CP (2020) Face stability analysis for a shield tunnel in anisotropic sands. Int J Geomech 20(5):04020043

Li J, Chen RP, Kong LG (2011) Model test study of the failure mechanism of shallow tunnels in dry sands (in Chinese). China Civil Eng J 044(007):142–148

Li JY, Liu W, Zou JJ et al (2018) Large-scale model tests on face instability of shallow shield tunnels in sand (in Chinese). Chin J Geotech Eng 40(03):562–567

Li W, Zhang CP, Tan ZB, Ma MS (2021) Effect of the seepage flow on the face stability of a shield tunnel. Tunn Undergr Space Technol 112:103900

Lin XT, Chen RP, Wu HN, Cheng HZ (2019) Three-dimensional stress-transfer mechanism and soil arching evolution induced by shield tunneling in sandy ground. Tunn Undergr Space Technol 93:103104

Ling XZ, Kong XX, Tang L et al (2021) Face stability of the slurry shield-driven tunnel with an impermeable filter cake in saturated medium sand. Arab J Geosci 14(15):1–11

Liu W, Zhao Y, Shi P et al (2018) Face stability analysis of shield-driven tunnels shallowly buried in dry sand using 1-g large-scale model tests. Acta Geotech 13(3):693–705

Liu HD, Zhang YF, Liu HN (2020a) Failure mechanism of face for slurry shield-driven tunnel in sand. KSCE J Civ Eng 24(1):3105–3118

Liu KQ, Ding WT, Chen R, Hou ML (2020b) Construction of three-dimensional failure model of shield tunnel face and calculation of the limit supporting force. Rock Soil Mech 41(7):1–12

Liu KQ, Dias D, Ding WT, Chen R (2021) Influence of soil-arching effect on tunnel face stability. Int J Geomech 21(7):04021107

Mair RJ, Taylor RN, Bracegirdleb A (1993) Subsurface settlement profiles above tunnels in clays. Géotechnique 43(2):315–320

Mollon G, Dias D, Soubra AH et al (2010) Face stability analysis of circular tunnels driven by a pressurized shield. J Geotech Geoenviron Eng 136(1):215–229

O'Reilly MP, New BM (1982) Settlement above tunnels in the United Kingdom—Their magnitude and prediction. Proceedings of tunnelling 82. Institution of Mining and Metallurgy, London, pp 173–181

Osman AS, Mair RJ, Bolton MD (2006) On the kinematics of 2D tunnel collapse in undrained clay. Géotechnique 56(9):585–595

Peck RB (1969) Deep excavations and tunneling in soft ground. Proceedings of the first international conference ISSMFE (Harvard). pp 225–290

Satyanarayana I, Budi G, Murmu S (2021) Stability analysis of a deep highwall slope using numerical modelling and statistical approach-a case study. Arab J Geosci 14:179

Sloan AW, Assadi A (1993) Stability of shallow tunnels in soft ground. In: Proc Wroth Memorial Symp., Thomas Thelford, London, 644–663

Soranzo E, Tamagnini R, Wu W (2015) Face stability of shallow tunnels in partially saturated soil: centrifuge testing and numerical analysis. Geotechnique 65(6):454–467

Sun XH, Miao LC, Lin HS (2017) Arching effect of soil ahead of working face in shield tunnel in sand with various depths (in Chinese). Rock Soil Mech 38(10):2980–2988

Wang J, He C, Xu GW (2019) Face stability analysis of EPB shield tunnels in dry granular soils considering dynamic excavation process. J Geotech Geoenviron 145:1–10

Zhang CP, Han KH, Zhang DL (2015) Face stability analysis of shallow circular tunnels in cohesive-frictional soils. Tunn Undergr Space Tech 50:345–357

Zhang CP, Li W, Zhu WJ, Tan ZB (2020) Face stability analysis of a shallow horseshoe-shaped shield tunnel in clay with a linearly increasing shear strength with depth. Tunn Undergr Space Tech 97:103291

Zhou XW, Pu JL (2002) Centrifuge model test on ground settlement induced by tunneling in sandy soil (in Chinese). Rock Soil Mech 23(5):1074–1079